Review of Scientific Instruments

CENTAUR—The small- and wide-angle neutron scattering diffractometer/ spectrometer for the Second Target Station of the Spallation Neutron Source

Cite as: Rev. Sci. Instrum. **93**, 075104 (2022); https://doi.org/10.1063/5.0090527
Submitted: 07 March 2022 • Accepted: 11 June 2022 • Published Online: 06 July 2022

Shuo Qian (钱朔), William Heller, Wei-Ren Chen, et al.

Review of Scientific Instruments ARTICLE scitation.org/journal/rsi

CENTAUR—The small- and wide-angle neutron scattering diffractometer/spectrometer for the Second Target Station of the Spallation Neutron Source

Cite as: Rev. Sci. Instrum. 93, 075104 (2022); doi: 10.1063/5.0090527
Submitted: 7 March 2022 • Accepted: 11 June 2022 •
Published Online: 6 July 2022

Shuo Qian (钱朔),[a] William Heller, Wei-Ren Chen, Andrew Christianson, Changwoo Do, Yangyang Wang, Jiao Y. Y. Lin, Thomas Huegle, Chenyang Jiang, Cristina Boone, Cameron Hart, and Van Graves

AFFILIATIONS

Oak Ridge National Laboratory, Oak Ridge, Tennessee 37830, USA

Note: Paper published as part of the Special Topic on New Science Opportunities at the Spallation Neutron Source Second Target Station.
[a]**Author to whom correspondence should be addressed:** qians@ornl.gov

ABSTRACT

CENTAUR has been selected as one of the eight initial instruments to be built at the Second Target Station (STS) of the Spallation Neutron Source at Oak Ridge National Laboratory. It is a small-angle neutron scattering (SANS) and wide-angle neutron scattering (WANS) instrument with diffraction and spectroscopic capabilities. This instrument will maximally leverage the high brightness of the STS source, the state-of-the-art neutron optics, and a suite of detectors to deliver unprecedented capabilities that enable measurements over a wide range of length scales with excellent resolution, measurements on smaller samples, and time-resolved investigations of evolving structures. Notably, the simultaneous WANS and diffraction capability will be unique among neutron scattering instruments in the United States. This instrument will provide much needed capabilities for soft matter and polymer sciences, geology, biology, quantum condensed matter, and other materials sciences that need *in situ* and *operando* experiments for kinetic and/or out-of-equilibrium studies. Beam polarization and a high-resolution chopper will enable detailed structural and dynamical investigations of magnetic and quantum materials. CENTAUR's excellent resolution makes it ideal for low-angle diffraction studies of highly ordered large-scale structures, such as skyrmions, shear-induced ordering in colloids, and biomembranes. Additionally, the spectroscopic mode of this instrument extends to lower momentum transfers than are currently possible with existing spectrometers, thereby providing a unique capability for inelastic SANS studies.

INTRODUCTION

In recent years, many fields of science have focused on understanding non-equilibrium kinetic processes in hierarchical complexes with both nanoscopic and macroscopic structures that matter to their property and function. Developing knowledge of such materials and processes is critical for establishing the scientific understanding necessary to enable various transformative opportunities mentioned in a number of recent reports from the US Department of Energy Basic Energy Sciences Advisory Committee, National Science Foundation, and National Academies of Sciences, Engineering and Medicine[1–3]—such as mastering hierarchical architectures and beyond-equilibrium matter; understanding heterogeneity, interfaces, and disorder beyond ideal materials and systems; and advancing imaging capabilities across multiple scales.

X ray and neutron scattering techniques have long contributed to our understanding of materials structures and dynamics at length scales that range from angstroms to micrometers. Neutrons have many unique properties, including sensitivity to light elements and a magnetic moment, which make neutron scattering techniques

indispensable research tools. In particular, neutron diffraction and small-angle neutron scattering (SANS) have provided fundamental insight about materials over length scales ranging from angstroms to hundreds of nanometers. Neutron diffraction excels at providing atomic-resolution structures of both small molecules and macromolecules, and SANS is ideally suited to probing long length scales in complex, disordered materials. Unfortunately, no existing neutron scattering instruments can investigate both structural regimes at the same time. To better capture the vastly different length scales, it is desirable to cover a much broader range of length scales with a single instrument using a single configuration, especially for those *in situ*, *operando*, and kinetics studies with conditions that are not easily duplicated or repeated. Furthermore, it is desirable to improve the temporal resolution of measurements from minutes to several seconds or to reduce the sample size significantly, which requires a high-flux neutron beam. A high-flux neutron beam also enables a raster-scan approach with a submillimeter-sized beam to map out nonuniform samples, thereby providing neutron imaging or tomography that uses the scattering and diffraction signal as a contrast mechanism, rather than the typical absorption signal used in radiography to understand the inhomogeneity in many engineering materials.[4–6]

With this capability gap in mind, the broader neutron scattering user community was consulted about what would be required of an instrument that served such a purpose. The desired instrument is a versatile and flexible SANS and wide-angle neutron scattering (WANS) instrument that has several unique features that enable new sciences. The key instrument parameters from various discussions are summarized in Table I and were used to develop an instrument called *CENTAUR*. CENTAUR is a small- and wide-angle neutron scattering diffractometer/spectrometer with a large dynamic range in reciprocal space. Specifically designed and optimized for the Second Target Station (STS) of the Spallation Neutron Source (SNS) at Oak Ridge National Laboratory (ORNL), it simultaneously covers length scales from atomic distance (diffraction) to hundreds of nanometers [small-angle scattering (SAS)]. Additionally, CENTAUR is also a direct geometry spectrometer that can probe dynamics at relatively large length-scale structures. Hence, the name "CENTAUR" was chosen to reflect the multi-functionality nature of the powerful future instrument.

In this paper, we present CENTAUR's specifications, features, and performance estimates. These particulars were developed using the following philosophy. First, as the only SANS-capable instrument selected for the first instrument suite at STS, it is an optimized SANS and WANS instrument with a minimum Q ($Q = 4\pi \sin\theta/\lambda$, where θ is half of the scattering angle and λ is the neutron wavelength) comparable to a typical high-performance SANS. Second, the expanded Q range reaches a diffraction regime comparable to that of a powder diffractometer. Third, it can be used as a direct geometry spectrometer by taking advantage of the time-of-flight high-flux source and SAS for inelastic SANS capability. The resulting instrument provides a truly unique capability to the scientific community.

CONCEPTUAL INSTRUMENT COMPONENT AND LAYOUT

There are three systems in the CENTAUR instrument concept necessary for achieving the desired requirements and flexibility: a variable optics system, a neutron detection system with large detector coverage with fixed location, and a high-speed chopper for spectroscopic analysis. The variable optics system with removable straight neutron guides—similar to other traditional SANS instruments, such as Bio-SANS[7] and GP-SANS[8]—provides adjustable flux and divergence with different collimation lengths for achieving the optimal conditions for different experiments. The detector system on CENTAUR consists of four arrays of detectors at different and fixed locations relative to the sample position. In addition to a low-angle detector array and a mid-angle array, a higher-angle array and

TABLE I. Key instrument parameter requirements.

Q range	0.001–20 $Å^{-1}$
Q resolution ($\Delta Q/Q$)	Forward detectors (small- and wide-angle): <10% Backscattering detectors (diffraction): <1%
Time resolution	~1 s for some samples
Additional capability	Inelastic SANS spectrometer and polarized neutrons up to 0.4 $Å^{-1}$
Sample size	Typically, 1–10 mm in diameter, other shape possible (e.g., 4 × 8 mm^2 or smaller); minimum static sample in volume: ~100 μl
Sample environment	Wide range of sample environments with convenient access and expandability. Some examples are automatic in-line flow cell, liquid handling robot (e.g., pH titrating), temperature/pressure ramping, flow-through cell, humidity control, stroboscopic sample environment capability, other *in situ* cells as needed (e.g., stain and shear), closed-cycle refrigerators, low-temperature cryostats, including ^{3}He and dilution refrigerators, and magnets

the backscattering array provide WANS and diffraction region coverage, which is important for understanding the structures at much smaller scales than from a typical SANS instrument. By virtue of the broad wavelength band, CENTAUR can cover 0.001–20 $Å^{-1}$ in a single configuration—the first instrument of its kind in the United States to fill this important capability gap. The instrument can be turned into a direct geometry spectrometer by inserting a high-speed monochromatic chopper near the sample position. The small-angle detector array provides an inelastic SANS capability to analyze dynamics occurring in large-scale structures. The inelastic SANS setup further extends the capability of direct geometry spectrometers at the SNS.

CENTAUR will be equipped with a polarization setup for regular operation, a capability currently lacking at the ORNL SANS instrument suite.[9] With a spacious sample area and flexible optics systems, CENTAUR will host an array of sample environments—ranging from a high-throughput sample changer to high-field magnets and from *in situ*/*operando* devices simulating real-world processes to additional multi-modal probes parallel to neutron scattering. Together with the high-flux neutron beam offered by the new source, CENTAUR will become a "lab-on-beam" facility, offering an unparalleled tool for solving many science questions. We also leverage developments at the existing ORNL SANS instruments at the High Flux Isotope Reactor (HFIR) (i.e., Bio-SANS and GP-SANS) and the First Target Station (FTS) (i.e., EQ-SANS) of the SNS to complement CENTAUR's capabilities, including their sample environment devices and software tools,[10–13] which are in use or under development. As a workhorse instrument at STS, we envision CENTAUR as an integral part of the SNS/HFIR neutron scattering facilities. In this section, we describe the major components of CENTAUR, which are shown in Fig. 1 and listed in Table II.

Source and neutron delivery system

CENTAUR will be located at position ST06 in the STS instrument hall, which views a para-hydrogen tube moderator that is 3 cm in diameter. This compact source provides the high brightness needed for high incident beam flux and wide Q range coverage. The total length of the instrument—also a factor of determining the usable wavelength band—is set to be 35.5 m to balance the broad wavelength band and the largest sample-to-detector distance. The instrument bisector is perpendicular to the proton beam direction on the target, potentially reducing the high-energy neutron background. The straight guide that extracts neutrons from the moderator will start about 1 m from the face of the moderator and extend to chopper 1 through the moderator monolith.

Bandwidth-defining choppers, chopper 1 and chopper 2, run at 15 Hz, the same pulse frequency as the source, or 7.5 Hz in a pulse-skipping mode for a wider wavelength band. They are an STS large single-disk chopper and an STS large double-disk chopper, respectively. When the choppers operate at 15 Hz, a bandwidth of ~7.44 Å can be achieved—for example, neutrons from the 2–9.44 Å band [Fig. 2(a)]. Combined with the large angular coverage from the detector arrays, this wide bandwidth will provide a wide dynamic Q range and high flux. In the skipped-pulse mode of 7.5 Hz, a bandwidth of ~14.88 Å (e.g., 0.5–15.38 Å) is achievable [Fig. 2(b)], which will provide an impressive dynamic Q-range. An STS large T0

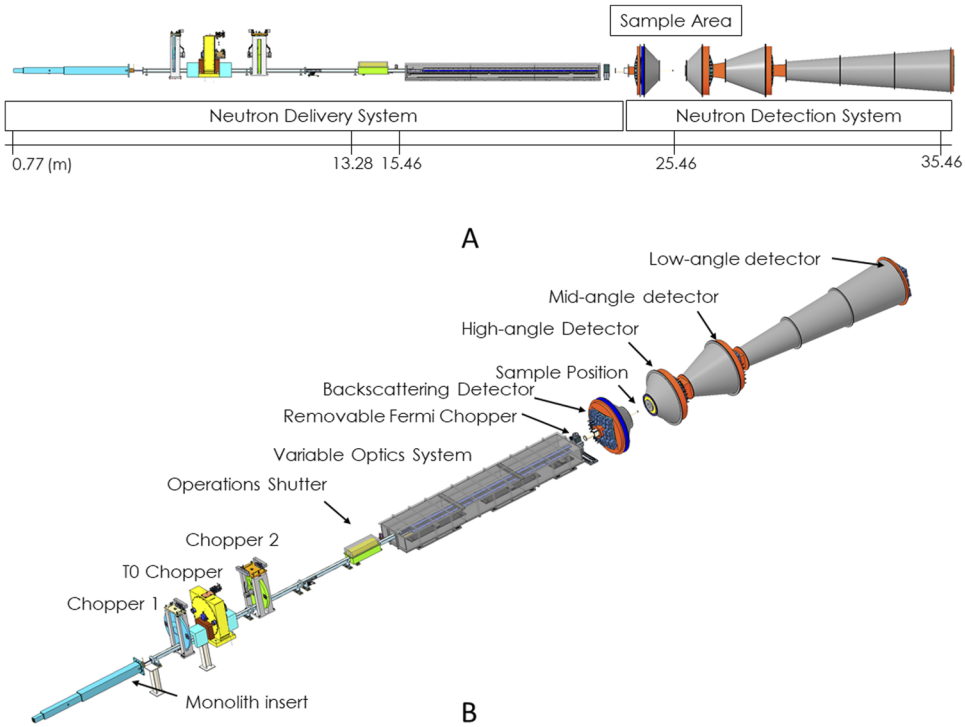

FIG. 1. Major components at CENTAUR. (a) A side view with various component distances relative to the source labeled. Once moderated in the moderator, neutrons enter the neutron delivery system to reach the sample area. The scattered neutrons are collected in the neutron detection system. (b) An isometric view with major components labeled. The colors are used to differentiate components in design drawing.

TABLE II. Primary CENTAUR instrument components and their locations.

Component	Description	Location from moderator
	Beam shaping and delivery	
Chopper 1	1 disk at 15 Hz	Z = 6.25 m (in bunker)
T0 chopper	1 rotor at 15 Hz	Z = 7.79 m (in bunker)
Chopper 2	2 disks at 15 Hz	Z = 9.69 m (in bunker)
Neutron guide	Straight guide, 3 × 3 cm^2, m = 3	Z = 1–22.5 m
Operations shutter	Heavy shutter	Z = 13.28 m
Variable optics box 1	Translatable out of beam	Z = 15.46 m
Variable optics box 2	Translatable out of beam	Z = 18.48 m
Variable optics box 3	Translatable out of beam	Z = 21.48 m
Fermi chopper	Translatable out of beam	Z = 22.71 m
Sample position		Z = 25.46 m
Component	Description	Location from sample
	Detector (R indicates a radial layout)	
Backscattering detector bank		R = −1.25 m
High-angle detector bank		R = +1.11 m
Mid-angle detector bank		R = +3.33 m
Low-angle detector bank		Z = +10 m

chopper will sit between chopper 1 and chopper 2 to reduce the fast neutrons and the prompt gamma ray pulse that results from the direct view of the moderator. This ensures more efficient transport of shorter wavelength neutrons, such as <2 Å, for diffraction and for high energy, low-angle spectroscopy while reducing the background noise. A straight guide in which a frame-overlap mirror is installed will extend from chopper 2 to the outer wall of the bunker at 13.288 m. The frame overlap mirror will remove undesired, long wavelength neutrons beyond the required band by eliminating the slow neutrons that arise from prior pulses, thereby improving the instrument spectrum and background.[14]

As required by STS, a maintenance shutter and an operations shutter are located next to the exterior wall of the target monolith and the target bunker, respectively. They will use standard STS designs.[15] The open configuration of both shutters will include integrated neutron guides for better neutron transport.

To provide different angular divergences, a variable optics system with interchangeable components, such as neutron guides, open space, and source-defining apertures, will be used. The system starts 15.46 m from the source. Inside the optics system, the first and the second collimation sections are 3 m in length, while the third one is 1 m in length. All neutron guides will be straight supermirrors (m = 3) with square openings of 3 × 3 cm^2 to match the source size. The variable optics system provides collimation lengths of 10, 7, 4, and 3 m (designated as the number of guides [NG] = 0, 1, 2, 3, respectively) to the nominal sample position, which is set 25.46 m away from the moderator. A polarizing supermirror will be in the first box as one of the removable optics components.

A Fermi chopper can be inserted with a translation stage at 22.71 m to perform spectroscopy. The Fermi chopper provides a monochromatic beam for performing direct geometry inelastic spectroscopy, particularly at low Q. An evacuated flight tube will extend from the end of the variable optics system to the nominal sample position.

The sample area

The nominal sample position, meaning that it is a reference point in the instrument geometry along with the moderator and the most frequently used sample position, will be at 25.46 m. It will be an open walk-in space inside a radiation-shielded hutch. Because SANS techniques are applicable for almost any sample state and morphology, it is very important that the sample area possess flexibility for accommodating sample holders and environments that range in size from cm to meters with minimum switch-over time. CENTAUR will offer flexibility and convenience for a broad range of sample environments, such as a robotic sample changer, cryo-magnets, or a ^{3}He analyzer for polarization analysis. There will be a second floor that provides convenient access for top-loading sample equipment, such as a cryo-magnet. The sample aperture is positioned immediately before the nominal sample position. A variable aperture system provides the flexibility to use different beam sizes, diameters typically from 1 to 10 mm, and additional shapes and sizes will also be available.

Neutron detection system

The large solid-angle coverage of the detector system is another central feature of CENTAUR. It provides a broad Q range in a single instrument configuration and improves operational efficiency by collecting as many of the scattered neutrons as possible to improve counting statistics and enable faster measurements. The

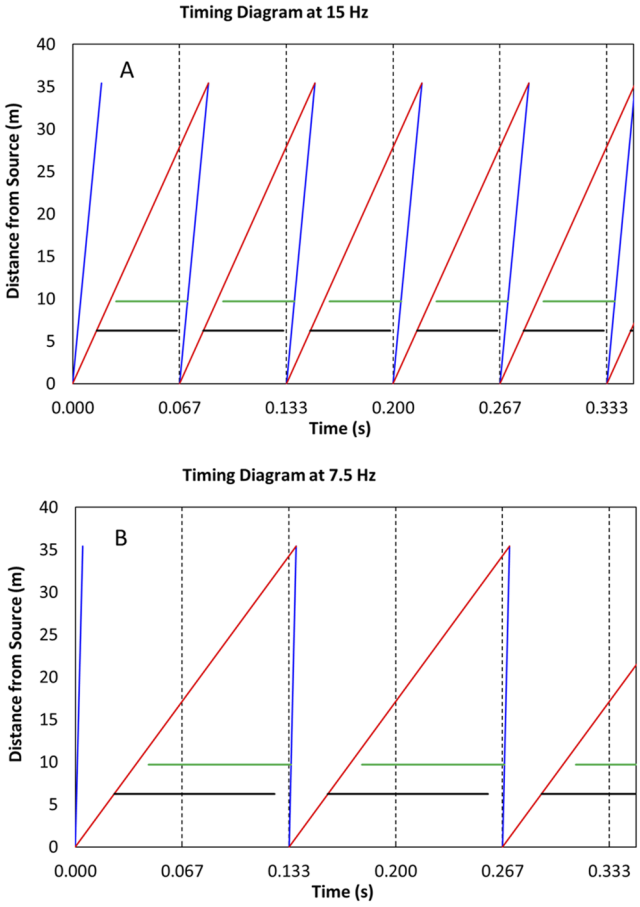

FIG. 2. Timing diagram examples for selected operation modes: (a) 15 Hz with a bandwidth of 2–9.44 Å and (b) 7.5 Hz with a bandwidth of 0.5–15.38 Å. The blue and red lines represent the shortest and the longest wavelengths, respectively, within the wavelength band defined by chopper 1 (black) and chopper 2 (green). The T0 chopper between them is not shown.

detectors will be scintillator Anger cameras with silicon photomultiplier (SiPM detector) modules that have a position resolution of 3×3 mm^2. With respect to the consideration of instrument geometry resolution, the pixel size is well-matched to the expected sample dimensions (1–10 mm diameter or square). Each module has an active area of 30×30 cm^2. In the forward direction, three banks of modules located at 10.00, 3.33, and 1.11 m from the nominal sample position will provide small- and wide-angle coverage with the overlapping Q range (Fig. 3). They are fixed in position, which will greatly increase measurement efficiency. An array of backscattering detectors located 1.25 m from the nominal sample position provides coverage in the very high Q diffraction regime. All detector banks except the low-angle bank are arranged with their surfaces tangent to a spherical surface with a radius equal to their distance from the nominal sample position. With the exception of the low-angle bank, the 3×3 arrays of detector modules in each bank are missing the center module to allow neutrons to pass through. The holes in the high-angle and the mid-angle arrays are optimized to

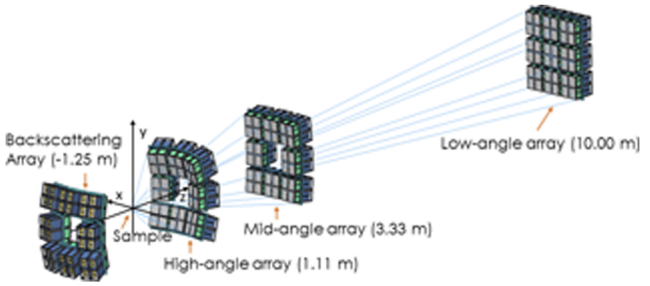

FIG. 3. Detector layout in the current preliminary design. The light blue lines illustrate how the rays from the sample position reach different detector arrays. The nominal sample position is shown, with the sample-to-detector distance labeled next to the detector arrays.

minimize shadowing onto the next array. The post-sample flight path for all forward scattering detectors is a vacuum vessel, whereas the backscattering detectors are in ambient air with an optional He gas-filled cover. Flat samples typically used for SANS experiments will enable more straightforward correction for the sample thickness during data reduction from the backscattering detectors compared with, for example, detector banks positioned 90° to the neutron beam direction.

In addition to typical beam traps of various sizes for blocking the direct beam before reaching the detector, semi-transparent ones will also be provided for simultaneous collection of scattered and transmitted neutron beams through the sample, which greatly simplifies measurement.

Polarization system

The neutron's magnetic moment is a major advantage of neutron scattering. Currently, none of the ORNL SANS instruments provide a polarized beam. CENTAUR will fill this gap. The polarization system provides the capability to separate incoherent scattering and nuclear scattering or magnetic scattering and nuclear scattering. Based on the feedback from the scientific user community, the required Q range for polarization analysis is 0.002 to 0.3 Å^{-1} under a magnetic field higher than 1 T. The system consists of these major components (Fig. 4). First, it includes a neutron spin supermirror polarizer with a 3×3 cm^2 cross section located in the first section of the variable optics system. Its m = 4 will ensure efficient reflection of neutron wavelengths longer than 2 Å. Second, an adiabatic fast passage spin flipper flips the neutron beam polarization relative to the magnetic field applied to the sample located just before the sample position. A magnetic guide field is integrated into the variable collimation system. The third component is a polarized ^{3}He neutron spin analyzer after the sample position to measure the polarization of the scattered neutron. For simplicity and practicality, especially in reducing the instrument background from auxiliary equipment, an *ex situ* system will be used.[16] In the *ex situ* system, multiple ^{3}He cells with different diameters of up to 15 cm can be dropped in and swapped easily during the experiment as needed. For example, with a 70% ^{3}He polarization ratio, the ^{3}He cell can be optimized to provide a good balance between the neutron transmission ratio and polarization ratio within the wavelength band. The compactness of the

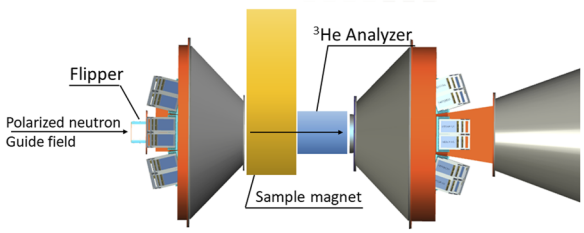

FIG. 4. The conceptual setup of the polarization system at CENTAUR. The *ex situ* ^{3}He analyzer cell (the blue box) will be placed in the sample area after sample environment, for example, an sample magnet system shown in yellow here. All components can be easily removed if not needed.

ex situ system will also provide improved magnetic shielding and additional distance from the sample environment magnet stray field. A "hot swap" during experiments into the polarized mode to quickly check signals is possible, as well as a subsequent return to the unpolarized mode for enhanced scattering intensity. With a 15 cm ^{3}He cell and a wavelength band of 2–9.44 Å at NG = 0, CENTAUR can provide a Q coverage of ~0.0016–0.5 Å^{-1}.

With the basic polarization setup and the spacious sample area, spin-echo modulated SANS (SEMSANS) measurements can be made using Wollaston prisms and an additional high-resolution detector with a position resolution of 0.2 mm placed in front of the central detector module of the low-angle bank to provide measurements covering size scales up to 10 μm, thereby further extending the capabilities of the instrument.[17,18]

INSTRUMENT PERFORMANCE EVALUATION

Instrument simulations were performed using Monte Carlo packages (McStas[19] or MCViNE[20,21]). The positions of the components are as described in the previous section (Conceptual Instrument Component and Layout). At present, no component exists for the T0 choppers to be used at the STS. As a result, the position was left as an empty gap in the Monte Carlo model. As mentioned previously, for maximum compatibility between the instrument's diffraction and SANS/WANS capabilities, a flat sample geometry was selected as the primary test sample geometry during the performance simulations. The flat sample geometry is broadly recommended for future experiments due to the ease afforded during data reduction, but other geometries are certainly feasible if the experiment necessitates it.

Q range and flux on sample

CENTAUR's detector arrangement and the broad wavelength band afford the ability to simultaneously measure a much wider Q range than in a typical SANS instrument. At 15 Hz, the gap in angular coverage between the forward scattering detectors and the backscattering detectors presents limitations on the wavelength bands that allow overlap in Q space. Therefore, it is recommended that the minimum wavelength setting be set at least 2 Å. During operation at 7.5 Hz, the large overlap in Q space between the forward and backscattering detectors is maintained over a wider range of minimum wavelength settings.

Flux estimates at the sample position for representative configurations at both potential operating frequencies were calculated from the McStas[19] simulations that assumed a 15-mm radius aperture and a 5-mm radius sample aperture and are presented in Table III. Additional simulations demonstrated that the spatial distribution of the flux within the radius of the sample is quite uniform. As can be seen in Tables III and S1, the flux at those configurations is very good compared to the existing ORNL SANS instruments,[9] as well as other instruments in operation and construction. Note that this might not be a fair comparison because the source characteristics are very different among a reactor cold source, FTS, and STS, but it shows that STS is an excellent source for a broader useable wavelength, especially cold neutrons. For the lowest Q, 0.001 Å^{-1} is reachable with neutrons around 16 Å. As the flux at longer wavelengths is comparable to HFIR monochromatic reactor SANS instruments, the performance at this Q point is comparable to Bio-SANS and GP-SANS. With orders-of-magnitude improvement in both flux and Q range, CENTAUR will be capable of time-resolved measurements of kinetic processes and covering a wide range of hierarchical structures, as mentioned in the desired specifications from the sciences cases discussed in the Science Examples section.

Estimated diffraction Q resolution of the backscattering

A flat, plate-like pseudo-polycrystalline sample with a thickness of 1 mm was used in a McStas simulation to estimate the diffraction Q resolution measured with the backscattering detector bank located at a 1.25 m radius sphere from the sample. The number of neutron guides used in simulations was set to NG = 0 and NG = 3. Both modes of operation were tested, 15 Hz (wavelength band 2–9.44 Å) and 7.5 Hz (wavelength band 0.50–15.36 Å). The simulated time-of-flight data collected on the detectors were converted into Q space, as shown in Fig. 5. The sample was defined to have evenly spaced, sharp diffraction peaks with the same intensity in the form of δ functions at Q values up to 15 Å^{-1}. The Q resolution was estimated from the ratio between the full width at half maximum (FWHM) of the diffracted peaks and the peak location, $\Delta Q/Q$. From the results, $\Delta Q/Q$ was found to be less than 1% in the backscattering detectors, satisfying the science requirement (Fig. S1).

Direct geometry spectrometer instrument performance evaluation

By taking advantage of the time-of-flight source, CENTAUR can be transformed to serve as a direct geometry spectrometer by inserting a high-speed chopper before the sample position, as described in the key instrument components. The high-speed chopper, which is expected to be a Fermi chopper, will select the monochromatic incident energy. The inelastic scattering from samples will be collected with the existing detector banks and analyzed by using the time-of-flight, effectively turning CENTAUR into a direct geometry inelastic spectrometer that can measure both structure and dynamics. The low-angle detector bank, at 10 m away from the nominal sample position, will provide a unique inelastic SANS capability among SNS instruments for measuring very small energy and momentum transfers. The instrument's dynamic range

TABLE III. CENTAUR Q range and flux at sample at selected instrument configurations with a source-defining aperture of 15 mm in radius and a sample aperture of 5 mm in radius based on the STS source file *BL6-Tube-90D-STS-Min-2G-source_mctal-55_sp.dat* (2021). The Q range from the forwarding detectors (three banks combined) and backscattering detectors is listed separately. The Q range is calculated by using corresponding scattering angle 2θ with λ_{min} and λ_{max} for Q_{max} and Q_{min}, respectively.

Configuration	Wavelength range (Å)	Q-range ($Å^{-1}$) (forwarding detectors)	Q range ($Å^{-1}$) (backscattering detector)	Flux at sample ($n\ s^{-1}\ cm^{-2}$)
15 Hz, NG = 0	2.00–9.44	0.0016–1.9	1.4–6.25	7.17×10^7
15 Hz, NG = 1	2.00–9.44	0.0023–1.9	1.4–6.25	1.39×10^8
15 Hz, NG = 2	2.00–9.44	0.0039–1.9	1.4–6.25	4.03×10^8
15 Hz, NG = 3	2.00–9.44	0.0056–1.9	1.4–6.25	6.89×10^8
15 Hz, NG = 3	1.00–8.44	0.0063–3.8	1.25–13.50	7.63×10^8
7.5 Hz, NG = 0	0.50–15.36	0.001–5.86	0.83–25.0	4.24×10^7
7.5 Hz, NG = 3	0.50–15.36	0.0035–5.86	0.83–25.0	3.99×10^8

in momentum transfer (Q) and energy transfer ($\Delta E = E_i - E_f$) is calculated in the range of incident energy 0.5–500 meV (12–0.4 Å), as shown in Fig. 6.

The performance as a spectrometer was simulated with MCViNE.[21] The instrument was set to use all neutron guides (NG = 3, the source-to-sample distance ~3 m) to maximize flux at the sample position. The burst time of the high-speed chopper was set to ~30 μs, providing a moderate energy resolution for the incident energy with decent flux at sample. Using samples with fixed momentum transfer and energy transfer, the inelastic scattering data were collected at the 10 m detector bank and then reduced into momentum transfer (Q) vs energy transfer ($\Delta E = E_i - E_f$). The instrument resolution at different incident energies (E_i = 80, 5 meV) was, then, obtained by measuring the FWHM of the inelastic peak in the Q–ΔE plot (Fig. 6). The result was consistent with calculations from the inelastic resolution equation[22] with a nominal detection uncertainty time, as shown by the dashed line in Figs. 6(b) and 6(c).

CENTAUR in relation to other SANS instruments

Driven by the need of the scientific community, SANS instruments at other leading neutron scattering facilities have extended their Q coverage for both minimum and maximum Q, as well as the dynamic range measured with a single configuration. Many recently commissioned and planned SANS instruments cover a Q range beyond a traditional SANS instrument by providing WANS and diffraction capabilities, such as Sans2d, LOQ, and LARMOR instruments at the ISIS Neutron and Muon Source; upcoming LoKI[23] and SKADI[24] instruments at the European Spallation Source (ESS); the VSANS instrument at the NIST Center for Neutron Research;[25]

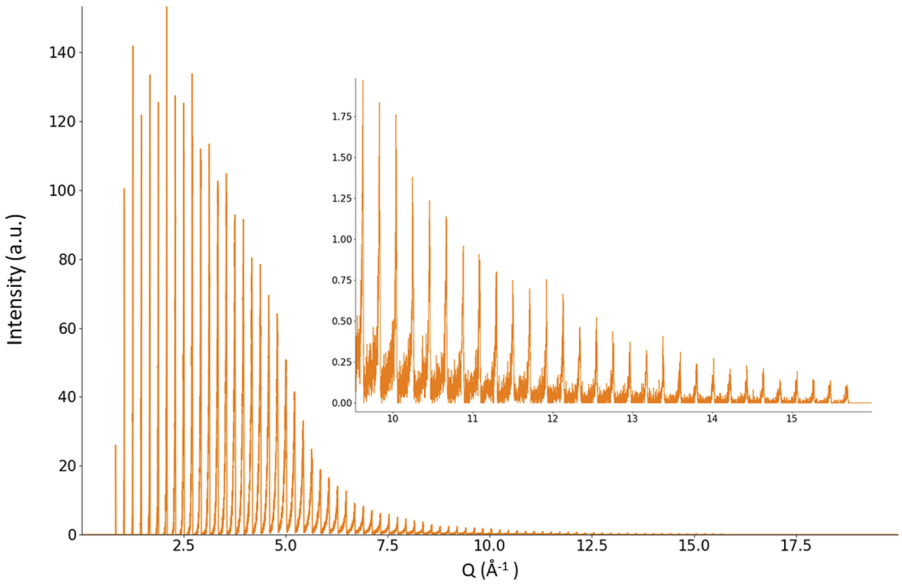

FIG. 5. Diffraction peaks collected at 7.5 Hz, NG = 3 on the backscattering detector array. The inset enlarges on the higher Q region. The 2D detector data were only circularly averaged into 1D profile without additional normalization and correction.

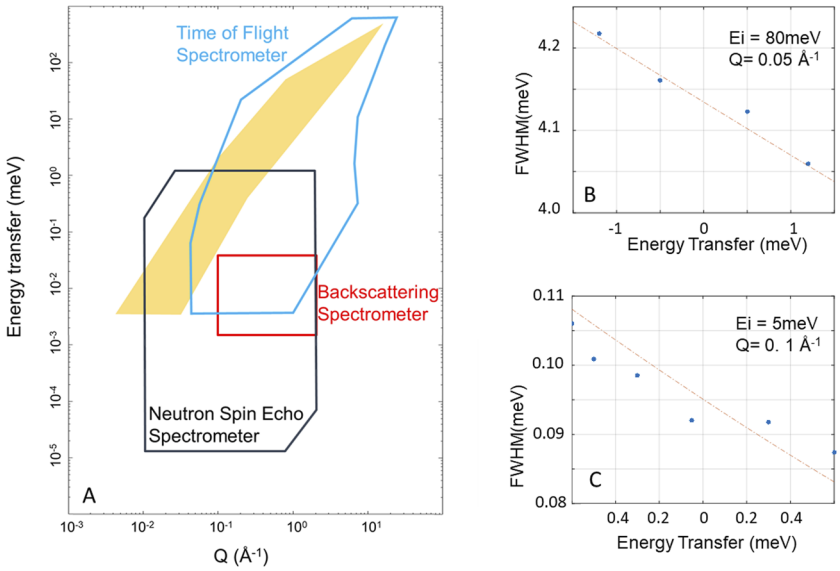

FIG. 6. (a) The dynamic range covered by using the CENTAUR 10 m detector is shown in yellow. For comparison, typical dynamic ranges from other neutron spectrometers, including neutron spin echo, backscattering, and time-of-flight spectrometers, are overlaid. (b) and (c) The inelastic energy resolution from MCViNE simulation at the 10 m detector bank at various incident energies (E_i) as labeled. The dots represent the MCViNE simulation; the dashed line is calculated from the inelastic resolution function from Ref. 22.

and the TAIKAN and iMATERIA instruments at the Japan Proton Accelerator Research Complex (J-PARC). Among them, TAIKAN covers up to 20 $Å^{-1}$ with its backscattering detector setup and relatively short minimum wavelength to 0.5 Å and serves as one of chief inspirations for CENTAUR. At the other extreme in Q, many SANS instruments are being developed to be capable of very-small angle neutron scattering that reaches a minimum Q of less than 0.001 $Å^{-1}$. Potentially, with a few modules of higher resolution detectors near the beam center and focusing optics, such as converging collimation slits,[26] CENTAUR can be upgraded to provide an improved minimum Q to achieve VSANS. The variable optics system at CENTAUR provides the flexibility and space for such an upgrade. However, considering the current science drivers, especially the much-needed flux for better time-resolved experiments and smaller samples, such capabilities are not presently considered for inclusion in the construction of CENTAUR.

It is worth noting that the suite of ORNL SANS instruments offers a wide range of capabilities that can be optimally configured for different experiment needs. For more static measurements, the Ultra-Small-Angle Neutron Scattering (USANS)[27] instrument on BL-1A at SNS provides a minimum Q as low as 10^{-5} $Å^{-1}$, and GP-SANS at HFIR provides 0.0007 $Å^{-1}$. Bio-SANS at HFIR and EQ-SANS at SNS provide SANS/WANS capabilities via various configurations. However, with the increase of orders in the flux and dynamic Q range, CENTAUR will provide much better time resolution or smaller samples while covering an even wider dynamic Q range at once, thereby filling a capacity gap for combining SANS and diffraction at SNS. Specifications from selected major SANS instruments are listed in Table S1of the supplementary material.

SCIENCE EXAMPLES

Neutron scattering's highly penetrating power, unique contrast especially among hydrogen isotopes, lack of radiation damage to samples, and magnetic moment have made it an indispensable tool for solving scientific questions in the structures and dynamics of complex materials across a large range of length and time scales. In this section, we provide a selection of science examples for which CENTAUR will provide high impacts. During the conceptualization of CENTAUR, many requirements were derived from some of these science examples. Although the science fields will rapidly evolve during the upcoming instrument design and construction phase, CENTAUR's higher performance and flexibility represent a generational improvement over existing instruments, and it will satisfy future emerging scientific needs.

Polymer sciences

Polymers dynamically self-assemble through processes that span six orders of magnitude of time (from seconds to days) into hierarchical structural length scales ranging from angstroms to micrometers. This multiscale assembly process determines both the structure and the properties of the material, including mechanical strength, conductivity, and biological activity. Unfortunately, current analytical techniques allow for only a small window of simultaneous observation that often does not encompass all the relevant features and processes of interest. CENTAUR, with its wide Q range and time-resolved capability, can cover the length scales in this observational range from angstrom to beyond 100 nm and time scales from seconds to days in a single measurement, thus providing the insight needed to correlate the hierarchical structure progression with the material's assembly mechanism. For example, we envision that CENTAUR can be applied to understand the bioinspired peptoid diblock helical assembly, which involves many length scales of hierarchical structure.[28–31] The result will help us understand how the lamellae stack to form helices and give rise to chirality.

Another application is the structure of polymer gels and networks (e.g., double network hydrogels,[32] slide-ring gels,[33] and polymer networks with mechanochemistry and mechanophores

properties[32,34–36]) that are essential in the development of many technologies. In particular, with an extremely wide Q range and temporal resolution of seconds, CENTAUR enables *in situ* structural characterization of transitions and the response of these materials to mechanical deformation that can quantify chain conformation at the individual chain level within hydrogels, which is a key measurement necessary to differentiate among modernized mechanical property theories for networks.[36–39] In addition, CENTAUR enables researchers to study a ubiquitous and practically important phenomenon in the industrial processing of polymers, such as flow-induced mixing, demixing, and phase transition. Many out-of-equilibrium phenomena can be studied with CENTAUR—including enhanced concentration fluctuations in semi-dilute solutions and polymer blends, phase separation in critical polymeric mixtures, and flow-induced polymer crystallization.[40–46]

Advanced manufacturing

Compared with the traditional manufacturing process, advanced manufacturing (AM) is unique in that its processing is often highly nonequilibrium. Thus, the properties of the built materials are process dependent. Understanding the nonequilibrium processes at the individual part and assembled device level to ensure consistency poses significant challenges to the wide-ranging adoption of AM technologies. Neutron scattering is a favorable tool because it is highly penetrable in many materials, including various metals.[47,48] CENTAUR—with its wide range in the reciprocal space (e.g., 0.001 to 20 $Å^{-1}$)—covers the length-scales involved in large phase separations, precipitates, and atomic deformations or stresses. The time resolution of seconds aligns closely with *in situ* structural investigation requirements. CENTAUR can address these challenges from emerging AM technologies beyond metals, including other materials such as ceramics and cement that share many common characterization challenges with metal AM at the part level.

Geosciences

Natural geological materials are continuously evolving, and their interactions with fluids and gases must be characterized at multiple scales and under *in situ* conditions as time elapses. Leveraged with the contrast variation provided by neutrons, CENTAUR extends previous studies of pore accessibility,[49–51] induced pore deformation,[52–55] and gas behaviors in pores[55–57] at the nanoscale to the atomic scale of the mineral structure, covering more length and time scales. In addition, a wide range of sample environments, temperature/pressure ramping, humidity control, strain, and shear extend the studies to probe much wider parameter space conditions that a truly high-throughput instrument can offer. For example, CENTAUR can be used to understand the dynamic processes of natural gas hydrate (NGH) formulation and disassociation. NGHs are considered an alternative fossil fuel energy resource because there are large deposits in permafrost and on the ocean floor.[58] Gas hydrates are also considered as a natural medium for gas storage[59] and for CO_2 capture and separation, therefore a carbon-neutral energy solution.[60] CENTAUR enables researchers to study the morphological evolution of the host geomaterials, the dynamics of gas–water transport and phase alteration, and the reactive potential between the fluid and host materials from the atomic scale to mesoscale length scales in a temporally resolved manner.

With its spectroscopic capability, CENTAUR can also help understand liquid dynamics in confined environments. For example, the relaxation dynamics of water in the confinement caused by interfacial water can be measured by using neutron and x-ray Brillouin scattering.[61,62] The inelastic SANS capability at CENTAUR will extend them further into a lower Q–E range to capture the low Q phonon dispersion and decay, as the understanding requires high-energy resolution over a wide Q range.

Biological systems

SAS techniques have become an important tool in structural biology, especially in the context of a functional complex or under physiologically relevant conditions. As the high-resolution structures of individual proteins are more available than ever with the development of computationally driven structure methods, such as AlphaFold[63] and RoseTTaFold,[64] SAS is poised to contribute to the understanding of more complex interactions between different biomolecules. At the same time, intrinsically disordered proteins (IDPs) or intrinsically disordered regions (IDRs) in proteins are highly dynamic, without well-defined structures. Such systems still present a difficulty for many other methods, even though the importance of IDPs/IDRs becomes more evident. Here, CENTAUR can provide valuable ensemble structural information. With higher flux, CENTAUR reduces the sample amount for biological samples, lowering the primary barrier presented to many biological experiments. The improved time-resolution allows us to understand many kinetic processes *in vitro* or even *in vivo*. For example, this could be useful in understanding the liquid–liquid phase separation process with a protein called the fused in sarcoma (FUS), which is involved in amyotrophic lateral sclerosis (ALS), an incurable neurodegenerative disorder that results in loss of voluntary muscle movement. CENTAUR will facilitate time-resolved studies of the structural transitions in FUS that occur over time at resolutions up to seconds, providing insights into the molecular-level details of these kinetics processes. Furthermore, once pathological aggregates or amyloid fibrils are formed, those highly ordered structures can be detected by the diffraction capability of CENTAUR to provide sub-nanometer structural information, without moving samples to another instrument. The large range of length scales covered by CENTAUR and the selective deuteration of samples will make it possible to detect conformational changes in specific molecules within complex surroundings and then report on the formation of larger ensembles/aggregates and responses to ligand binding, unfolding, allosterically driven organizational changes, and other processes under physiologically relevant conditions.[65–67] In addition, SANS is a powerful method for studying protein–DNA complexes and protein–protein assemblies using the neutron contrast matching technique.[68–70] CENTAUR enables automated contrast variation-size exclusion chromatography-SANS with a flow-through setup, exchanging the buffer with different ratios of H_2O/D_2O for more routine analysis of protein–nucleic acid assemblies.

Another science example is biomembrane systems. Biomembranes are an important part of cell biology yet are very difficult complex to study. Neutron scattering including SANS

provides greater understanding in biomembranes, enabling the rational design of antimicrobial drugs that penetrate or disrupt envelopes of pathogenic microbes,[71–73] the design of functional biomimetic membranes,[74–76] the development of a predictive understanding of first-line microbial responses to external environmental perturbations, and the engineering of microbial membranes to improve their tolerance of the stressful conditions associated with biofuel/bioproduct formation.[77] In particular, a smaller beam with high flux and the much-improved instrument resolution will make CENTAUR well-suited for grazing-incidence membrane diffraction to resolve atomic structure features in biomembranes. Lamellar and nonlamellar diffraction have provided detailed bilayer structures with important physiological relevance, such as membrane fusion, membrane pore formation, membrane–protein interaction, and biomembrane-based biosensors.[78–81] Membrane diffraction is usually performed at dedicated diffractometers requiring ranges from relatively low Q (e.g., ~0.03 $Å^{-1}$) to reach large unit cells of up to 200 Å and to maximum Q up to 2.0 $Å^{-1}$—a range well covered by CENTAUR.

The wide accessible Q range of CENTAUR will allow for the synchronous acquisition of both SANS and WANS for the needed length scales to better understand pharmaceutical agents, such as protein therapeutics and mRNA vaccines with lipid nanoparticles, which have grown into major classes of medicines. For example, with the reduced intermolecular distances in protein therapeutics, a variety of non-specific protein–protein interactions (PPIs) can take place, including hydrogen bonding and electrostatic and hydrophobic forces.[82] Most other biophysical characterization methods are not suitable for measuring concentrated protein samples, and the prediction of the colloidal stability of protein from dilute solutions is often found to be inappropriate.[83–85] However, CENTAUR provides a powerful, nondestructive characterization tool for measuring such a sample under those needed conditions.[85]

Quantum condensed matter

A traditional strength of magnetic SANS is the investigation of flux lattices of superconductors and chiral magnetism, including the celebrated skyrmion spin textures.[86,87] The high flux and high resolution of CENTAUR will enable such experiments to be completed quickly and with a new level of precision. However, the primary benefit of CENTAUR will be to create several new directions in this field. The first crucial gain is the ability to resolve relatively small moments making up large length-scale spin textures while simultaneously separating features that may be unresolvable at reactor-based SANS experiments, which typically use large $\Delta\lambda/\lambda$ or sacrifice flux for smaller $\Delta\lambda/\lambda$. The advent of high-throughput entropic mapping of field and temperature space in candidate magnetic materials[88,89] has revealed a host of unexplained states; many of these are proposed to be previously hidden topological spin textures, which are likely distinguishable from one another and from topologically trivial spin configurations only though subtle variations in SANS data that CENTAUR can provide. The high flux and high throughput ability of CENTAUR can rapidly traverse the magnetic and temperature phase space of small-volume crystals, thus providing a breakthrough for the community. Furthermore, the broad Q range of CENTAUR will open new possibilities for investigating newly predicted spin textures, such as antiferromagnetic skyrmions,[90] which are not accessible with current SANS instrumentation. The second crucial gain is that CENTAUR will also enable a key new window into understanding the emergent electrodynamics of these spin textures, many of which are sought for potential applications. In this case, understanding the response to time-varying electric and magnetic fields is essential. The time structure of the STS neutron pulse provides an ideal pathway to investigate the dynamics of current and applied field.

A fundamental goal of spectroscopic investigations of magnetic materials is to determine the effective spin Hamiltonian, which is the underlying origin of the physical behavior. CENTAUR's ability to resolve energy transfer will enable investigations of spin dynamics in the first Brillouin zone in magnetic materials. The only current implementation of a similar capability at a modern high-flux spallation source is the High-Resolution Chopper (HRC) spectrometer at J-PARC.[91] With CENTAUR's much lower-angular coverage compared with a typical direct geometry spectrometer[92,93] and the broad wavelength band (a wide incident neutron energy range), the dynamic range will be extended into a much lower Q range with reasonably good energy resolution. The inelastic SANS capability will enhance the understanding of ferromagnets, ferromagnetic quantum criticality,[94] and excitations of mesoscale spin textures,[95] and it will enable the dynamics of magnetic nanoparticles to be probed.

OUTLOOK

Complemented by the significant gain in the new neutron source at STS, CENTAUR will allow users to perform *in situ* characterizations of the temporal evolution of metastable structures on a routine basis. The proposed instrument will form the backbone for research with neutrons for several fields of growing interest: it will enable the study of kinetic processes and nonequilibrium problems in soft materials subjected to external forces and stimuli in new detail. With smaller sample volumes and an in-line sample flow system integrated with an apparatus, such as a size-exclusion column or liquid-handing robot, CENTAUR will provide researchers with higher sample-related data quality and/or much higher throughput—currently major barriers for many neutron scattering experiments. As CENTAUR's design and construction progress in the upcoming years, we will also take advantage of new developments using artificial intelligence methods for instrument operation and data analysis. Along with a new suite of spectrometers such as BWAVES,[96] CHESS,[92,97] and EXPANSE[98] at STS, CENTAUR will provide transformative new capabilities for many sciences.

SUPPLEMENTARY MATERIAL

See the supplementary material for an additional table (Table S1) with specifications from selected major SANS instruments and $\Delta Q/Q$ measured from the diffraction of the pseudo-polycrystalline sample on the backscattering detector (Fig. S1).

ACKNOWLEDGMENTS

The authors thank Dr. Rachel Segalman, Dr. Yun Liu, Dr. Kushol Gupta, Dr. Zimei Bu, Dr. Bradley Olsen, Dr. Stephen Wilson, and Dr. Morten Eskildsen for being part of the CENTAUR proposal

team and contributing to the success of the instrument selection. The authors also thank Dr. Wei Chen, Dr. Richard Kriwacki, Dr. Richard Gillilan, Dr. Shimin Liu, Dr. Rui Zhang, Dr. Koichi Mayumi, Dr. Amy Y. Xu, Dr. Fan Zhang, Dr. Jeffrey J. Richards, Dr. Kathryn Krycka, Dr. Lilin He, and Dr. Chelsea Chen for discussions.

This research used resources of the Spallation Neutron Source at the Second Target Station Project at ORNL. A portion of this research used resources at the Spallation Neutron Source, a DOE Office of Science User Facility operated by ORNL. ORNL is managed by UT-Battelle LLC for DOE's Office of Science. Work by Andrew Christianson was supported by DOE, Office of Science, Basic Energy Sciences, Materials Sciences and Engineering Division.

AUTHOR DECLARATIONS

Conflict of Interest

The authors have no conflicts to disclose.

Author Contributions

Shuo Qian (钱 朔)**:** Conceptualization (equal); Data curation (lead); Formal analysis (lead); Investigation (lead); Project administration (lead); Supervision (lead); Visualization (lead); Writing – original draft (lead); Writing – review & editing (lead). **William Heller:** Conceptualization (equal); Formal analysis (equal); Investigation (equal); Writing – original draft (supporting); Writing – review & editing (equal). **Wei-Ren Chen:** Conceptualization (equal). **Andrew Christianson:** Conceptualization (equal); Writing – original draft (supporting); Writing – review & editing (supporting). **Changwoo Do:** Conceptualization (equal); Writing – original draft (supporting); Writing – review & editing (supporting). **Yangyang Wang:** Conceptualization (equal). **Jiao Y. Y. Lin:** Investigation (supporting); Methodology (supporting); Software (equal); Validation (supporting). **Thomas Huegle:** Formal analysis (supporting); Investigation (supporting); Methodology (supporting); Software (equal); Visualization (supporting). **Chenyang Jiang:** Conceptualization (equal); Investigation (supporting). **Cristina Boone:** Project administration (equal); Resources (equal); Visualization (lead). **Cameron Hart:** Investigation (equal); Methodology (equal); Resources (equal); Visualization (equal). **Van Graves:** Methodology (equal); Project administration (equal); Resources (equal); Visualization (equal).

DATA AVAILABILITY

The data that support the findings of this study are available from the corresponding author upon reasonable request.

REFERENCES

[1]National Academies of Sciences Engineering Medicine, Frontiers of Materials Research: A Decadal Survey, 2019.

[2]NSF, Frontiers in Polymer Science and Engineering (Workshop Report), NSF, AFRL/AFOSR, ARO, DOE/BES, FDA, NIST, ONR, 2016.

[3]Challenges at the Frontiers of Matter and Energy: Transformative Opportunities for Discovery Science, A Report from the Basic Energy Sciences Advisory Committee, U.S. DOE, 2015.

[4]F. Schaff, M. Bech, P. Zaslansky, C. Jud, M. Liebi, M. Guizar-Sicairos, and F. Pfeiffer, "Six-dimensional real and reciprocal space small-angle X-ray scattering tomography," Nature **527**(7578), 353–356 (2015).

[5]T. A. Grünewald, M. Liebi, N. K. Wittig, A. Johannes, T. Sikjaer, L. Rejnmark, Z. Gao, M. Rosenthal, M. Guizar-Sicairos, H. Birkedal, and M. Burghammer, "Mapping the 3D orientation of nanocrystals and nanostructures in human bone: Indications of novel structural features," Sci. Adv. **6**(24), eaba4171 (2020).

[6]E. R. Louden, A. W. D. Leishman, C. Rastovski, S. J. Kuhn, L. DeBeer-Schmitt, C. D. Dewhurst, N. D. Zhigadlo, and M. R. Eskildsen, "Structural studies of metastable and equilibrium vortex lattice domains in MgB_2," New J. Phys. **21**(6), 063003 (2019).

[7]W. T. Heller, V. S. Urban, G. W. Lynn, K. L. Weiss, H. M. O'Neill, S. V. Pingali, S. Qian, K. C. Littrell, Y. B. Melnichenko, M. V. Buchanan, D. L. Selby, G. D. Wignall, P. D. Butler, and D. A. Myles, "The Bio-SANS instrument at the High Flux Isotope Reactor of Oak Ridge National Laboratory," J. Appl. Crystallogr. **47**(4), 1238–1246 (2014).

[8]G. D. Wignall, K. C. Littrell, W. T. Heller, Y. B. Melnichenko, K. M. Bailey, G. W. Lynn, D. A. Myles, V. S. Urban, M. V. Buchanan, D. L. Selby, and P. D. Butler, "The 40 m general purpose small-angle neutron scattering instrument at Oak Ridge National Laboratory," J. Appl. Crystallogr. **45**(5), 990–998 (2012).

[9]W. T. Heller, M. Cuneo, L. Debeer-Schmitt, C. Do, L. He, L. Heroux, K. Littrell, S. V. Pingali, S. Qian, C. Stanley, V. S. Urban, B. Wu, and W. Bras, "The suite of small-angle neutron scattering instruments at Oak Ridge National Laboratory," J. Appl. Crystallogr. **51**(2), 242–248 (2018).

[10]X. Yao, B. Avery, M. Bobrek, L. Debeer-Schmitt, X. Geng, R. Gregory, G. Guyotte, M. Harrington, S. Hartman, L. He, L. Heroux, K. Kasemir, R. Knudson, J. Kohl, C. Lionberger, K. Littrell, M. Pearson, S. V. Pingali, C. Pratt, S. Qian, M. Ruiz-Rodriguez, V. Sedov, G. Taufer, V. Urban, and K. Vodopivec, "A unified user-friendly instrument control and data acquisition system for the ORNL SANS instrument suite," Appl. Sci. **11**(3), 1216 (2021).

[11]W. T. Heller, "Tools for visualization and analysis of small-angle neutron scattering data: Descriptions and examples," Report No. ORNL/TM-2022/1497, Oak Ridge National Laboratory (ORNL), Oak Ridge, TN, 2022.

[12]W. T. Heller, J. Hetrick, J. Bilheux, B. Calvo, W.-R. Chen, L. DeBeer-Schmitt, C. Do, M. Doucet, M. R. Fitzsimmons, W. F. Godoy, G. E. Granroth, S. Hahn, L. He, F. Islam, J. Lin, K. C. Littrell, M. McDonnell, J. McGaha, P. F. Peterson, S. V. Pingali, S. Qian, A. T. Savici, Y. Shang, C. B. Stanley, V. S. Urban, R. E. Whitfield, C. Zhang, W. Zhou, J. J. Billings, M. J. Cuneo, F. Leal, T. Wang, and B. Wu, "**drtsans**: the data reduction toolkit for small-angle neutron scattering at Oak Ridge National Laboratory," SoftwareX **19**, 101101 (2022).

[13]W. T. Heller, M. Doucet, and R. K. Archibald, "*Sas-temper*: Software for fitting small-angle scattering data that provides automated reproducibility characterization," SoftwareX **16**, 100849 (2021).

[14]J. K. Zhao, C. Y. Gao, and D. Liu, "The extended *Q*-range small-angle neutron scattering diffractometer at the SNS," J. Appl. Crystallogr. **43**(5), 1068–1077 (2010).

[15]Neutron Sciences Directorate, STS Instruments Conceptual Design 15 Hz Chopper Models (STS04-41-IN0002-RA), Oak Ridge National Laboratory, 2018.

[16]T. Wang, C. Y. Jiang, T. O. Farmer, L. Debeer-Schmitt, J. F. Wenzel, L. McDonald, J. L. Robertson, M. R. Fitzsimmsons, and X. Tong, "New polarized small angle neutron scattering capability at the High Flux Isotope Reactor," Physica B **551**, 492–495 (2018).

[17]J. Schmitt, J. J. Zeeuw, J. Plomp, W. G. Bouwman, A. L. Washington, R. M. Dalgliesh, C. P. Duif, M. A. Thijs, F. Li, R. Pynn, S. R. Parnell, and K. J. Edler, "Mesoporous silica formation mechanisms probed using combined spin–echo modulated small-angle neutron scattering (SEMSANS) and small-angle neutron scattering (SANS)," ACS Appl. Mater. Interfaces **12**(25), 28461–28473 (2020).

[18]F. Li, S. R. Parnell, H. Bai, W. Yang, W. A. Hamilton, B. B. Maranville, R. Ashkar, D. V. Baxter, J. T. Cremer, and R. Pynn, "Spin echo modulated small-angle neutron scattering using superconducting magnetic Wollaston prisms," J. Appl. Crystallogr. **49**(1), 55–63 (2016).

[19]P. Willendrup, E. Farhi, E. Knudsen, U. Filges, and K. Lefmann, "McStas: Past, present and future," J. Neutron Res. **17**(1), 35–43 (2014).

[20]J. Y. Y. Lin, H. L. Smith, G. E. Granroth, D. L. Abernathy, M. D. Lumsden, B. Winn, A. A. Aczel, M. Aivazis, and B. Fultz, "MCViNE—An object oriented

Monte Carlo neutron ray tracing simulation package," Nucl. Instrum. Methods Phys. Res., Sect. A **810**, 86–99 (2016).
[21]J. Y. Y. Lin, F. Islam, G. Sala, I. Lumsden, H. Smith, M. Doucet, M. B. Stone, D. L. Abernathy, G. Ehlers, J. F. Ankner, and G. E. Granroth, "Recent developments of MCViNE and its applications at SNS," J. Phys. Commun. **3**(8), 085005 (2019).
[22]G. Ehlers, A. A. Podlesnyak, J. L. Niedziela, E. B. Iverson, and P. E. Sokol, "The new cold neutron chopper spectrometer at the Spallation Neutron Source: Design and performance," Rev. Sci. Instrum. **82**(8), 085108 (2011).
[23]A. Jackson and K. Kanaki, "LoKI-A broad band high flux SANS instrument for the ESS," in Proceedings of the 21st Meeting of the International Collaboration on Advanced Neutron Sources, 2015.
[24]S. Jaksch, A. Chennevière, S. Désert, T. Kozielewski, H. Feilbach, P. Lavie, R. Hanslik, A. Gussen, S. Butterweck, R. Engels, H. Frielinghaus, S. Förster, and P. Müller-Buschbaum, "Technical specification of the small-angle neutron scattering instrument SKADI at the European Spallation Source," Appl. Sci. **11**(8), 3620 (2021).
[25]J. Barker, J. Moyer, S. Kline, G. Jensen, J. Cook, C. Gagnon, E. Kelley, J. P. Chabot, N. Maliszewskyj, C. Parikh, W. Chen, R. P. Murphy, and C. Glinka, "The very small angle neutron scattering instrument at the National Institute of Standards and Technology," J. Appl. Crystallogr. **55**(2), 271–283 (2022).
[26]S. Abbas, S. Désert, A. Brûlet, V. Thevenot, P. Permingeat, P. Lavie, and J. Jestin, "On the design and experimental realization of a multislit-based very small angle neutron scattering instrument at the European Spallation Source," J. Appl. Crystallogr. **48**(4), 1242–1253 (2015).
[27]M. Agamalian, L. Heroux, K. C. Littrell, and J. M. Carpenter, "Progress on the time-of-flight ultra small angle neutron scattering instrument at SNS," J. Phys.: Conf. Ser. **1021**(1), 012033 (2018).
[28]H. K. Murnen, A. M. Rosales, J. N. Jaworski, R. A. Segalman, and R. N. Zuckermann, "Hierarchical self-assembly of a biomimetic diblock copolypeptoid into homochiral superhelices," J. Am. Chem. Soc. **132**(45), 16112–16119 (2010).
[29]J. J. L. M. Cornelissen, M. Fischer, N. A. J. M. Sommerdijk, and R. J. M. Nolte, "Helical superstructures from charged poly(styrene)-poly(isocyanodipeptide) block copolymers," Science **280**(5368), 1427–1430 (1998).
[30]C.-K. Chen, S.-C. Lin, R.-M. Ho, Y.-W. Chiang, and B. Lotz, "Kinetically controlled self-assembled superstructures from semicrystalline chiral block copolymers," Macromolecules **43**(18), 7752–7758 (2010).
[31]R.-M. Ho, M.-C. Li, S.-C. Lin, H.-F. Wang, Y.-D. Lee, H. Hasegawa, and E. L. Thomas, "Transfer of chirality from molecule to phase in self-assembled chiral block copolymers," J. Am. Chem. Soc. **134**(26), 10974–10986 (2012).
[32]J. P. Gong, Y. Katsuyama, T. Kurokawa, and Y. Osada, "Double-network hydrogels with extremely high mechanical strength," Adv. Mater. **15**(14), 1155–1158 (2003).
[33]Y. Okumura and K. Ito, "The polyrotaxane gel: A topological gel by figure-of-eight cross-links," Adv. Mater. **13**(7), 485–487 (2001).
[34]A. L. Black, J. M. Lenhardt, and S. L. Craig, "From molecular mechanochemistry to stress-responsive materials," J. Mater. Chem. **21**(6), 1655–1663 (2011).
[35]E. Ducrot, Y. Chen, M. Bulters, R. P. Sijbesma, and C. Creton, "Toughening elastomers with sacrificial bonds and watching them break," Science **344**(6180), 186–189 (2014).
[36]M. Zhong, R. Wang, K. Kawamoto, B. D. Olsen, and J. A. Johnson, "Quantifying the impact of molecular defects on polymer network elasticity," Science **353**(6305), 1264–1268 (2016).
[37]J. Ramirez, T. J. Dursch, and B. D. Olsen, "A molecular explanation for anomalous diffusion in supramolecular polymer networks," Macromolecules **51**(7), 2517–2525 (2018).
[38]A. A. Gusev, "Numerical estimates of the topological effects in the elasticity of Gaussian polymer networks and their exact theoretical description," Macromolecules **52**(9), 3244–3251 (2019).
[39]M. Lang, "On the elasticity of polymer model networks containing finite loops," Macromolecules **52**(16), 6266–6273 (2019).
[40]M. Tirrell, "Phase behavior of flowing polymer mixtures," Fluid Phase Equilib. **30**, 367–380 (1986).
[41]R. G. Larson, "Flow-induced mixing, demixing, and phase transitions in polymeric fluids," Rheol. Acta **31**(6), 497–520 (1992).
[42]M. Doi and A. Onuki, "Dynamic coupling between stress and composition in polymer solutions and blends," J. Phys. II **2**(8), 1631–1656 (1992).
[43]S. T. Milner, "Dynamical theory of concentration fluctuations in polymer solutions under shear," Phys. Rev. E **48**(5), 3674–3691 (1993).
[44]H. Ji and E. Helfand, "Concentration fluctuations in sheared polymer solutions," Macromolecules **28**(11), 3869–3880 (1995).
[45]A. Onuki, "Phase transitions of fluids in shear flow," J. Phys.: Condens. Matter **9**(29), 6119 (1997).
[46]N. Jiang, T. Yu, O. A. Darvish, S. Qian, I. K. Mkam Tsengam, V. John, and D. Zhang, "Crystallization-driven self-assembly of coil–comb-shaped polypeptoid block copolymers: Solution morphology and self-assembly pathways," Macromolecules **52**(22), 8867–8877 (2019).
[47]F. Zhang, L. Chen, and D. Bhattacharyya, "In situ synchrotron and neutron characterization of additively manufactured alloys," JOM **73**(1), 174–176 (2021).
[48]T. H. Kang, B. G. Compton, W. T. Heller, S. Qian, G. S. Smith, V. S. Urban, C. E. Duty, and C. Do, "Potentials with small-angle neutron scattering technique for understanding structure–property relation of 3D-printed materials," Polym. Eng. Sci. **59**(s2), E65–E70 (2019).
[49]C. R. Clarkson, N. Solano, R. M. Bustin, A. M. M. Bustin, G. R. L. Chalmers, L. He, Y. B. Melnichenko, A. P. Radliński, and T. P. Blach, "Pore structure characterization of North American shale gas reservoirs using USANS/SANS, gas adsorption, and mercury intrusion," Fuel **103**, 606 (2012).
[50]L. F. Ruppert, R. Sakurovs, T. P. Blach, L. He, Y. B. Melnichenko, D. F. R. Mildner, and L. Alcantar-Lopez, "A USANS/SANS study of the accessibility of pores in the Barnett shale to methane and water," Energy Fuels **27**(2), 772–779 (2013).
[51]R. Zhang, S. Liu, J. Bahadur, D. Elsworth, Y. Melnichenko, L. He, and Y. Wang, "Estimation and modeling of coal pore accessibility using small angle neutron scattering," Fuel **161**, 323–332 (2015).
[52]G. Sang, S. Liu, D. Elsworth, R. Zhang, and M. Bleuel, "Pore-scale water vapor condensation behaviors in shales: An experimental study," Transp. Porous Media **135**(3), 713–734 (2020).
[53]S. Liu and R. Zhang, "Anisotropic pore structure of shale and gas injection-induced nanopore alteration: A small-angle neutron scattering study," Int. J. Coal Geol. **219**, 103384 (2020).
[54]R. Zhang, S. Liu, A. San-Miguel, R. Schweins, S. Le Floch, and V. Pischedda, "Nanoscale coal deformation and alteration of porosity and pore orientation under uniaxial compression: An in situ SANS study," Rock Mech. Rock Eng. **54**, 3593 (2021).
[55]K. L. Stefanopoulos, T. G. A. Youngs, R. Sakurovs, L. F. Ruppert, J. Bahadur, and Y. B. Melnichenko, "Neutron scattering measurements of carbon dioxide adsorption in pores within the marcellus shale: Implications for sequestration," Environ. Sci. Technol. **51**(11), 6515–6521 (2017).
[56]A. P. R. Eberle, H. E. King, P. I. Ravikovitch, C. C. Walters, G. Rother, and D. J. Wesolowski, "Direct measure of the dense methane phase in gas shale organic porosity by neutron scattering," Energy Fuels **30**(11), 9022–9027 (2016).
[57]Y. B. Melnichenko, *Small-Angle Scattering from Confined and Interfacial Fluids: Applications to Energy Storage and Environmental Science* (Springer International Publishing, 2016).
[58]X.-S. Li, C.-G. Xu, Y. Zhang, X.-K. Ruan, G. Li, and Y. Wang, "Investigation into gas production from natural gas hydrate: A review," Appl. Energy **172**(C), 286–322 (2016).
[59]S. Takeya, H. Mimachi, and T. Murayama, "Methane storage in water frameworks: Self-preservation of methane hydrate pellets formed from NaCl solutions," Appl. Energy **230**, 86 (2018).
[60]Z. W. Ma, P. Zhang, H. S. Bao, and S. Deng, "Review of fundamental properties of CO_2 hydrates and CO_2 capture and separation using hydration method," Renewable Sustainable Energy Rev. **53**, 1273–1302 (2016).
[61]F. Sette, G. Ruocco, M. Krisch, U. Bergmann, C. Masciovecchio, V. Mazzacurati, G. Signorelli, and R. Verbeni, "Collective dynamics in water by high energy resolution inelastic x-ray scattering," Phys. Rev. Lett. **75**(5), 850–853 (1995).
[62]E. Mamontov, A. De Francesco, F. Formisano, A. Laloni, L. Sani, B. M. Leu, A. H. Said, and A. I. Kolesnikov, "Water dynamics in a lithium chloride aqueous solution probed by Brillouin neutron and x-ray scattering," J. Phys.: Condens. Matter **24**(6), 064102 (2012).
[63]J. Jumper, R. Evans, A. Pritzel, T. Green, M. Figurnov, O. Ronneberger, K. Tunyasuvunakool, R. Bates, A. Žídek, A. Potapenko, A. Bridgland, C. Meyer, S. A. A. Kohl, A. J. Ballard, A. Cowie, B. Romera-Paredes, S. Nikolov, R. Jain, J. Adler, T. Back, S. Petersen, D. Reiman, E. Clancy, M. Zielinski, M. Steinegger,

M. Pacholska, T. Berghammer, S. Bodenstein, D. Silver, O. Vinyals, A. W. Senior, K. Kavukcuoglu, P. Kohli, and D. Hassabis, "Highly accurate protein structure prediction with AlphaFold," Nature **596**(7873), 583–589 (2021).
[64]M. Baek, F. DiMaio, I. Anishchenko, J. Dauparas, S. Ovchinnikov, G. R. Lee, J. Wang, Q. Cong, L. N. Kinch, R. D. Schaeffer, C. Millán, H. Park, C. Adams, C. R. Glassman, A. DeGiovanni, J. H. Pereira, A. V. Rodrigues, A. A. van Dijk, A. C. Ebrecht, D. J. Opperman, T. Sagmeister, C. Buhlheller, T. Pavkov-Keller, M. K. Rathinaswamy, U. Dalwadi, C. K. Yip, J. E. Burke, K. C. Garcia, N. V. Grishin, P. D. Adams, R. J. Read, and D. Baker, "Accurate prediction of protein structures and interactions using a three-track neural network," Science **373**(6557), 871–876 (2021).
[65]Y. Wang, H. Zhou, E. Onuk, J. Badger, and L. Makowski, "What can we learn from wide-angle solution scattering?," in *Biological Small Angle Scattering: Techniques, Strategies and Tips*, Advances in Experimental Medicine and Biology, edited by B. Chaudhuri, I. G. Muñoz, S. Qian, and V. S. Urban (Springer, Singapore, 2017), pp. 131–147.
[66]S. Sparks, D. B. Temel, M. P. Rout, and D. Cowburn, "Deciphering the 'fuzzy' interaction of FG nucleoporins and transport factors using small-angle neutron scattering," Structure **26**(3), 477–484.E4 (2018).
[67]D. Anunciado, D. K. Rai, S. Qian, V. Urban, and H. O'Neill, "Small-angle neutron scattering reveals the assembly of alpha-synuclein in lipid membranes," Biochim. Biophys. Acta, Proteins Proteomics **1854**(12), 1881–1889 (2015).
[68]G. D. Van Duyne and K. Rutherford, "Large serine recombinase domain structure and attachment site binding," Crit. Rev. Biochem. Mol. Biol. **48**(5), 476–491 (2013).
[69]H. Li, R. Sharp, K. Rutherford, K. Gupta, and G. D. Van Duyne, "Serine integrase *att*P binding and specificity," J. Mol. Biol. **430**(21), 4401–4418 (2018).
[70]M. Bush, B. M. Alhanshali, S. Qian, C. B. Stanley, W. T. Heller, T. Matsui, T. M. Weiss, I. D. Nicholl, T. Walz, D. J. E. Callaway, and Z. Bu, "An ensemble of flexible conformations underlies mechanotransduction by the cadherin–catenin adhesion complex," Proc. Natl. Acad. Sci. U. S. A. **116**(43), 21545–21555 (2019).
[71]M. Zasloff, "Antimicrobial peptides of multicellular organisms," Nature **415**(6870), 389–395 (2002).
[72]B. P. Lazzaro, M. Zasloff, and J. Rolff, "Antimicrobial peptides: Application informed by evolution," Science **368**(6490), eaau5480 (2020).
[73]S. Qian, V. K. Sharma, and L. A. Clifton, "Understanding the structure and dynamics of complex biomembrane interactions by neutron scattering techniques," Langmuir **36**(50), 15189–15211 (2020).
[74]C. Hélix-Nielsen, "Biomimetic membranes as a technology platform: Challenges and opportunities," Membranes **8**(3), 44 (2018).
[75]J. M. Hutchison, K.-C. Shih, H. A. Scheidt, S. M. Fantin, K. F. Parson, G. A. Pantelopulos, H. R. Harrington, K. F. Mittendorf, S. Qian, R. A. Stein, S. E. Collier, M. G. Chambers, J. Katsaras, M. W. Voehler, B. T. Ruotolo, D. Huster, R. L. McFeeters, J. E. Straub, M.-P. Nieh, and C. R. Sanders, "Bicelles rich in both sphingolipids and cholesterol and their use in studies of membrane proteins," J. Am. Chem. Soc. **142**(29), 12715–12729 (2020).
[76]R. Guo, J. Sumner, and S. Qian, "Structure of diisobutylene maleic acid copolymer (DIBMA) and its lipid particle as a 'stealth' membrane-mimetic for membrane protein research," ACS Appl. Bio Mater. **4**(6), 4760–4768 (2021).
[77]Y. Qi, H. Liu, X. Chen, and L. Liu, "Engineering microbial membranes to increase stress tolerance of industrial strains," Metab. Eng. **53**, 24–34 (2019).
[78]S. Qian, W. Wang, L. Yang, and H. W. Huang, "Structure of transmembrane pore induced by Bax-derived peptide: Evidence for lipidic pores," Proc. Natl. Acad. Sci. U. S. A. **105**(45), 17379–17383 (2008).
[79]M. Kim, M. Porras-Gomez, and C. Leal, "Graphene-based sensing of oxygen transport through pulmonary membranes," Nat. Commun. **11**(1), 1103 (2020).
[80]S. Qian and D. K. Rai, "Grazing-angle neutron diffraction study of the water distribution in membrane hemifusion: From the lamellar to rhombohedral phase," J. Phys. Chem. Lett. **9**(19), 5778–5784 (2018).
[81]S. Qian and P. A. Zolnierczuk, "Interaction of a short antimicrobial peptide on charged lipid bilayer: A case study on aurein 1.2 peptide," BBA Adv. **2**, 100045 (2022).
[82]P. Garidel, M. Hegyi, S. Bassarab, and M. Weichel, "A rapid, sensitive and economical assessment of monoclonal antibody conformational stability by intrinsic tryptophan fluorescence spectroscopy," Biotechnol. J. **3**(9–10), 1201–1211 (2008).
[83]M. A. Woldeyes, W. Qi, V. I. Razinkov, E. M. Furst, and C. J. Roberts, "How well do low- and high-concentration protein interactions predict solution viscosities of monoclonal antibodies?," J. Pharm. Sci. **108**(1), 142–154 (2019).
[84]M. A. Blanco, T. Perevozchikova, V. Martorana, M. Manno, and C. J. Roberts, "Protein–protein interactions in dilute to concentrated solutions: α-Chymotrypsinogen in acidic conditions," J. Phys. Chem. B **118**(22), 5817–5831 (2014).
[85]A. Y. Xu, M. M. Castellanos, K. Mattison, S. Krueger, and J. E. Curtis, "Studying excipient modulated physical stability and viscosity of monoclonal antibody formulations using small-angle scattering," Mol. Pharm. **16**(10), 4319–4338 (2019).
[86]C. Back, V. Cros, H. Ebert, K. Everschor-Sitte, A. Fert, M. Garst, T. Ma, S. Mankovsky, T. L. Monchesky, M. Mostovoy, N. Nagaosa, S. S. P. Parkin, C. Pfleiderer, N. Reyren, A. Rosch, Y. Taguchi, Y. Tokura, K. von Bergmann, and J. Zang, "The 2020 skyrmionics roadmap," J. Phys. D: Appl. Phys. **53**(36), 363001 (2020).
[87]N. Nagaosa and Y. Tokura, "Topological properties and dynamics of magnetic skyrmions," Nat. Nanotechnol. **8**(12), 899–911 (2013).
[88]L. Kautzsch, J. D. Bocarsly, C. Felser, S. D. Wilson, and R. Seshadri, "Controlling Dzyaloshinskii-Moriya interactions in the skyrmion host candidates $FePd_{1-x}Pt_xMo_3N$," Phys. Rev. Mater. **4**(2), 024412 (2020).
[89]J. D. Bocarsly, R. F. Need, R. Seshadri, and S. D. Wilson, "Magnetoentropic signatures of skyrmionic phase behavior in FeGe," Phys. Rev. B **97**(10), 100404 (2018).
[90]S. Gao, H. D. Rosales, F. A. Gómez Albarracín, V. Tsurkan, G. Kaur, T. Fennell, P. Steffens, M. Boehm, P. Čermák, A. Schneidewind, E. Ressouche, D. C. Cabra, C. Rüegg, and O. Zaharko, "Fractional antiferromagnetic skyrmion lattice induced by anisotropic couplings," Nature **586**(7827), 37–41 (2020).
[91]S. Itoh, T. Yokoo, T. Masuda, H. Yoshizawa, M. Soda, S. Ibuka, Y. Ikeda, M. Yoshida, T. Hawai, D. Kawana, R. Sugiura, T. Asami, Y. Kawamura, T. Shinozaki, and Y. Ihata, "High resolution chopper spectrometer HRC and neutron Brillouin scattering," AIP Conf. Proc. **1969**(1), 050002 (2018).
[92]G. Sala, J. Y. Y. Lin, V. B. Graves, and G. Ehlers, "Conceptual design of CHESS, a new direct-geometry inelastic neutron spectrometer dedicated to studying small samples," J. Appl. Crystallogr. **51**(2), 282–293 (2018).
[93]M. B. Stone, J. L. Niedziela, D. L. Abernathy, L. DeBeer-Schmitt, G. Ehlers, O. Garlea, G. E. Granroth, M. Graves-Brook, A. I. Kolesnikov, A. Podlesnyak, and B. Winn, "A comparison of four direct geometry time-of-flight spectrometers at the Spallation Neutron Source," Rev. Sci. Instrum. **85**(4), 045113 (2014).
[94]T. R. Kirkpatrick and D. Belitz, "Ferromagnetic quantum critical point in noncentrosymmetric systems," Phys. Rev. Lett. **124**(14), 147201 (2020).
[95]N. Mohanta, A. D. Christianson, S. Okamoto, and E. Dagotto, "Signatures of a liquid-crystal transition in spin-wave excitations of skyrmions," Commun. Phys. **3**(1), 229 (2020).
[96]E. Mamontov, C. Boone, M. J. Frost, K. W. Herwig, T. Huegle, J. Y. Y. Lin, B. McCormick, W. McHargue, A. D. Stoica, P. Torres, and W. Turner, "A concept of a broadband inverted geometry spectrometer for the Second Target Station at the Spallation Neutron Source," Rev. Sci. Instrum. **93**(4), 045101 (2022).
[97]G. Sala *et al.*, "CHESS: The future direct geometry spectrometer at the Second Target Station," Rev. Sci. Instrum. **93**, 065109 (2022).
[98]C. Do, R. Ashkar, C. Boone, W.-R. Chen, and G. Ehlers, "EXPANSE: A time-of-flight expanded angle neutron spin echo spectrometer at the Second Target Station of the Spallation Neutron Source," Rev. Sci. Instrum. (Submitted) (2022).